



Department of Physics & Astronomy  
Experimental Particle Physics Group  
Kelvin Building, University of Glasgow,  
Glasgow, G12 8QQ, Scotland  
Telephone: +44 (0)141 339 8855 Fax: +44 (0)141 330 5881

GLAS-PPE/1999-06  
May 1999

## Structure of Real and Virtual Photons from ZEUS

N. Macdonald

### Abstract

Measurements sensitive to the structure of both real and virtual photons are presented and compared to theoretical models with various photon parton distribution functions (PDFs). Measurements for real photons show a tendency for the available photon PDFs to be too small to describe the data. For virtual photons, the photon PDF is seen to decrease with increasing photon virtuality. In order to describe the data, resolved photon processes are required up to a photon virtuality of at least  $4.5 \text{ GeV}^2$ .

# 1 Introduction

Experimental information on the partonic structure of the photon can be obtained from the data taken at the HERA ep collider experiments. Leading order (LO) QCD predicts that photon interactions have a two-component nature. In direct photon processes the entire momentum of the photon takes part in the hard subprocess with a parton from the proton whereas in resolved photon processes the photon acts as a source of partons and one of these enters the hard subprocess. By measuring inclusive dijet events (two or more jets) information on the structure of the real photon can be extracted. By also measuring the scattered electron, information can be obtained on the evolution of this structure as a function of the virtuality of the photon,  $Q^2$ .

The fraction of the photon's four momentum which enters the hard subprocess at leading order, denoted by  $x_\gamma^{LO}$ , is equal to unity for direct processes, and less than unity for resolved processes. Experimentally it is not possible to measure  $x_\gamma^{LO}$  directly. Instead, an observable quantity  $x_\gamma^{obs}$  is defined which is calculable and well-defined to all orders of perturbation theory.  $x_\gamma^{obs}$  is the fraction of the photon momentum manifest in the two highest transverse energy jets and is defined by the equation

$$x_\gamma^{obs} = \frac{\sum E_{Tj} e^{-\eta_j}}{2E_e y}$$

where  $E_{Tj}$  is the transverse energy of jet  $j$ ,  $\eta_j$  is the pseudorapidity of the jet measured in the lab frame, and  $y$  is the inelasticity of the event.

“Direct enriched” events are defined as being those with  $x_\gamma^{obs} > 0.75$  and “resolved enriched” events as those with  $x_\gamma^{obs} < 0.75$ . This value gives the optimal separation of the leading order direct and resolved event classes.

## 2 Dijets in Photoproduction and Real Photon Structure

The kinematic selection cuts made in order to examine the structure of the real photon are

- Two or more jets ( $k_T$  clustering algorithm)
- $Q^2 \simeq 0 \text{ GeV}^2$
- $E_T^{jet\ leading} > 14 \text{ GeV}$ ,  $E_T^{jet\ second} > 11 \text{ GeV}$
- $-1 < \eta^{jet} < 2$
- $0.20 < y < 0.85$

The advantages of using high  $E_T$  dijets are that they provide a hard scale where perturbative QCD (pQCD) is expected to work, the hadronisation corrections are small, and the effect of underlying events is small. Given these assumptions, the data can be compared directly to NLO pQCD calculations without the need to simulate some hadronisation model. This analysis concentrates on the high  $x_\gamma^{obs}$  region where the quark densities in the photon are not strongly constrained by  $e^+e^-$  experiments.

The measured ZEUS data is compared to NLO pQCD calculations for three photon PDFs, GRV-HO [4], AFG-HO [6] and GS96-HO [5]. The NLO calculations have been performed by three groups of theorists, Harris et al. [1], Klasen et al. [2] and Frixione et al. [3]. Since the agreement between the calculations is excellent only one of the calculations is plotted.

Figure 1 shows the differential dijet cross section as a function of  $E_T^{jet\ leading}$  for  $0.20 < y < 0.85$ . There is an excess in the data above theory for central jets ( $0 < \eta^{jet} < 1$ ) below an  $E_T$  of 25 GeV. The assumption that the hadronisation corrections are negligible is not true for backward jets ( $-1 < \eta^{jet} < 0$ ), so no conclusions are drawn about the backward region, rather the discrepancy between data and theory is ascribed to a theoretical uncertainty.

Figure 2 shows the cross section for a narrower range in  $y$ . This provides a better sensitivity to the photon structure since the cross section is no longer averaged over the broader  $y$  range. There is an excess in the data seen for central ( $0 < \eta^{jet} < 1$ ) and forward ( $1 < \eta^{jet} < 2$ ) jets, both for the whole  $x_\gamma^{obs}$  range and the high  $x_\gamma^{obs}$  range.

The excess in the data above theory for jets with  $E_T < 25 \text{ GeV}$  and for central and forward rapidities suggests that the available photon PDF parametrisations, based on  $e^+e^- F_2^\gamma$  data, are too small in this kinematic regime.

### 3 Ratio of Dijet Cross Sections vs $Q^2$

The kinematic selection cuts made for the analysis of virtual photons are

- Two or more jets ( $k_T$  clustering algorithm)
- $Q^2 \simeq 0$ ,  $0.1 < Q^2 < 0.55$ ,  $1.5 < Q^2 < 4.5$  ( $\text{GeV}^2$ )
- $0.20 < y < 0.55$
- $E_T^{jets} > 5.5$  GeV
- $-1.125 < \eta^{jets} < 2.2$

Three different  $Q^2$  regions are available for measurement.  $Q^2 \simeq 1.0$   $\text{GeV}^2$  corresponds to quasi-real photons, where the electron is not measured, and the large bulk of such events lead to a median  $Q^2$  of  $0.001$   $\text{GeV}^2$ . ZEUS has a small angle electron detector for tagging events in the transition region between photoproduction and DIS ( $0.1 < Q^2 < 0.55$   $\text{GeV}^2$ ). For  $1.5 < Q^2 < 4.5$   $\text{GeV}^2$  the electron is detected in the ZEUS main calorimeter.

Figure 3 shows the ratio of the resolved to the direct dijet cross sections as a function of  $Q^2$ . Since some of the systematic uncertainties cancel in the ratio, this is a more precise measurement than an absolute differential cross section. The data fall with increasing  $Q^2$ . This is compared to the dijet ratio obtained with HERWIG 5.9 [7] using a photon PDF which does not evolve with  $Q^2$  (GRV LO [8]) and one which does (SaS1D [10]). The HERWIG ratio with GRV LO is flat, while that obtained with SaS 1D falls with increasing  $Q^2$ . Therefore the fall of the ratio with  $Q^2$  observed in the data indicates that the data require a virtual photon PDF which evolves with photon virtuality. The LEPTO 6.5.1 [9] curve shows the prediction for leading order direct processes in DIS only. Note that this ratio is non-zero as may be understood given that LEPTO contains higher-order processes in the approximation of parton-showering and hadronization. The data approach this direct only limit, however resolved processes are still required in order to describe the data up to at least  $Q^2 = 4.5$   $\text{GeV}^2$ .

### References

- [1] B.W. Harris and J.F. Owens, *Phys. Rev.* **D56** (1997) 4007.
- [2] M. Klasen and G. Kramer, *Z. Phys* **C76** (1997) 67;  
M. Klasen, T. Kleinwort and G. Kramer, *Eur. Phys. J.* **C1** (1998) 1.
- [3] S. Frixione and G. Ridolfi, *Nucl. Phys.* **B507** (1997) 315;  
S. Frixione, *Nucl. Phys.* **B507** (1997) 295.
- [4] M. Glück, E. Reya and A. Vogt, *Phys. Rev.* **D45** (1992) 3986;  
M. Glück, E. Reya and A. Vogt, *Phys. Rev.* **D46** (1992) 1973.
- [5] L.E. Gordon and J.K. Storrow, *Nucl. Phys.* **B489** (1997) 405.
- [6] P. Aurenche, J. Guillet and M. Fontannaz, *Z. Phys* **C64** (1994) 621.
- [7] HERWIG 5.9; G. Marchesini et al., *Computer Phys. Comm.* **67** (1992) 465.
- [8] M. Glück, E. Reya and A. Vogt, *Phys. Rev.* **D46** (1992) 1973.
- [9] G. Ingelman, A. Edin and J. Rathsman, *Computer Phys. Comm.* **101** (1997) 108-134.
- [10] G. Schuler and T. Sjöstrand, *Phys. Lett.* **B376** (1996) 193.

# ZEUS 1995

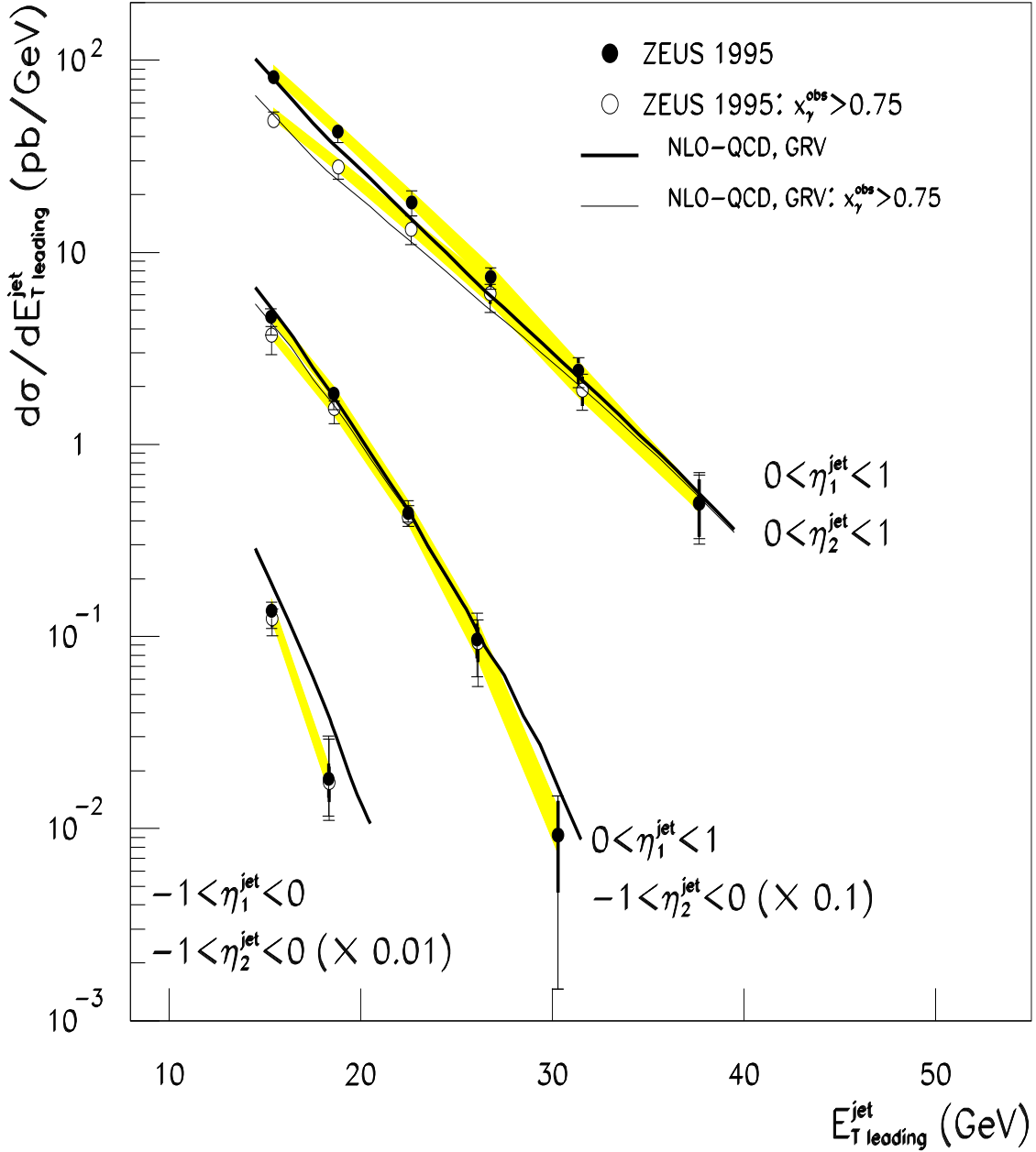
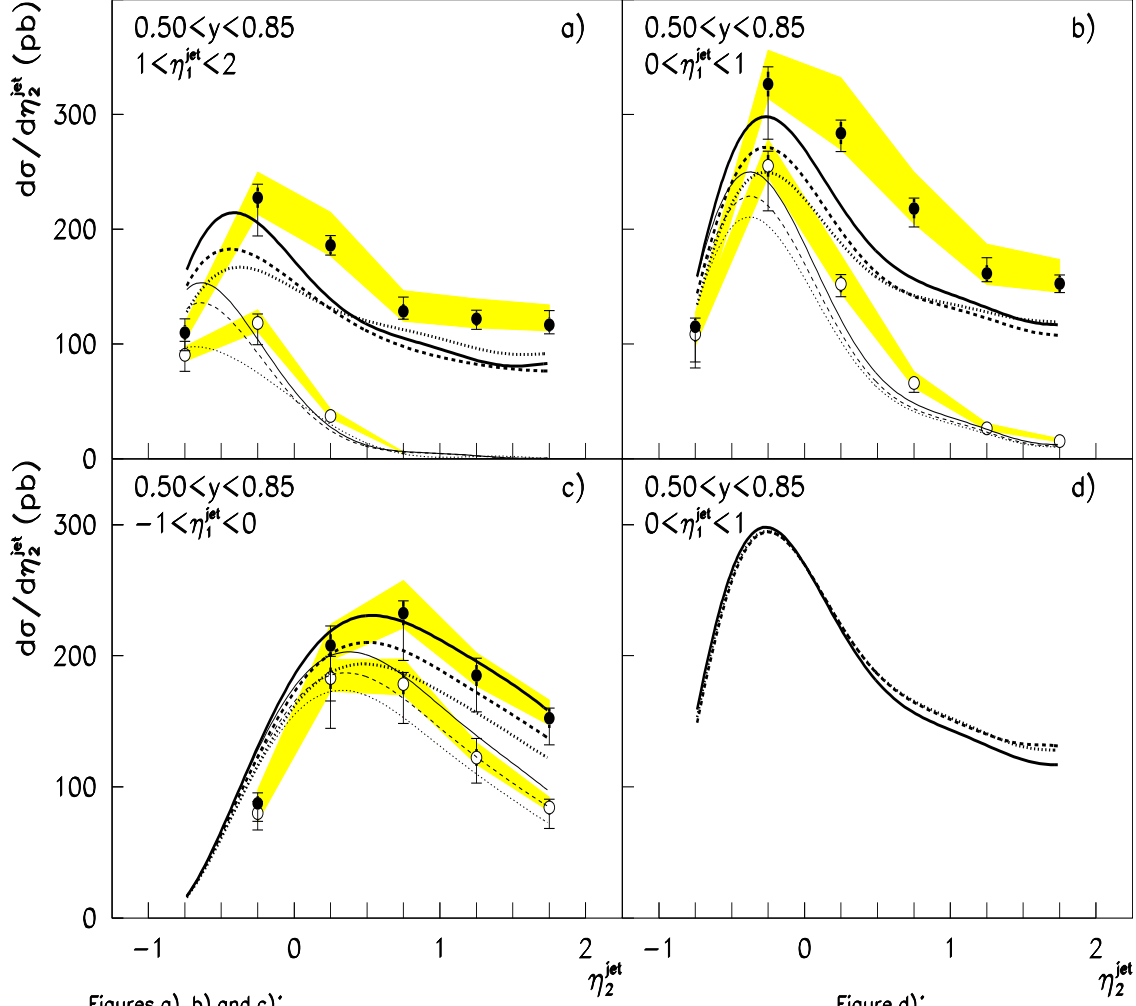


Figure 1: Differential dijet cross section as a function of  $E_{T \text{ leading}}^{jet}$  for  $0.20 < y < 0.85$ .

## ZEUS 1995



Figures a), b) and c):

- ZEUS 1995
- ZEUS 1995,  $x_7^{obs} > 0.75$
- NLO-QCD, GRV-HO
- NLO-QCD, GRV-HO,  $x_7^{obs} > 0.75$
- ..... NLO-QCD, AFG-HO
- ..... NLO-QCD, AFG-HO,  $x_7^{obs} > 0.75$
- ..... NLO-QCD, GS96-HO
- ..... NLO-QCD, GS96-HO,  $x_7^{obs} > 0.75$

Figure d):

- HARRIS et al., GRV-HO
- ..... KLASSEN et al., GRV-HO
- ..... FRIXIONE et al., GRV-HO

Figure 2: Differential dijet cross section as a function of  $\eta_2^{jet}$  in bins of  $\eta_1^{jet}$  for  $0.50 < y < 0.85$ .

# ZEUS PRELIMINARY 1995

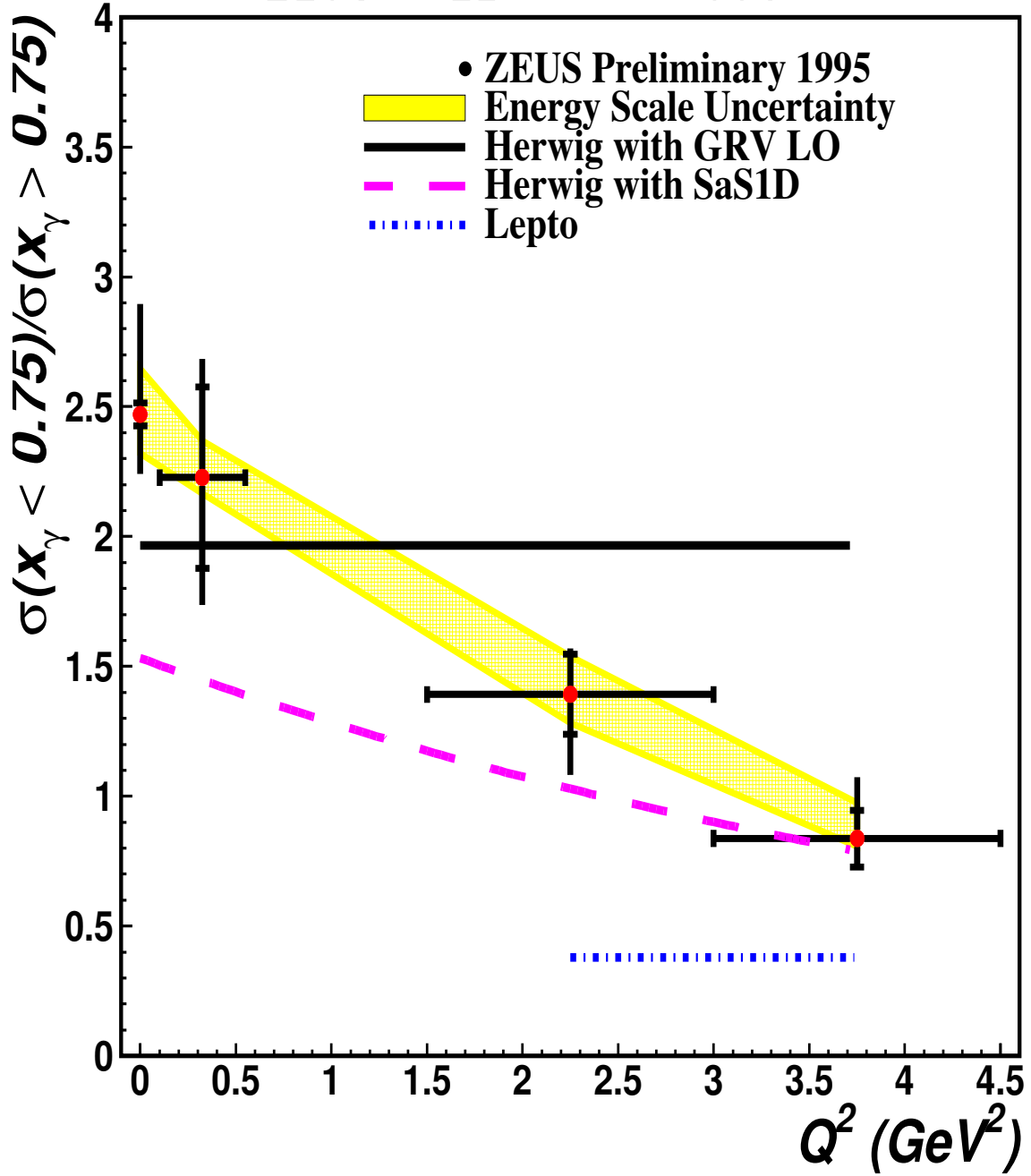


Figure 3: Ratio of resolved enriched to direct enriched dijet cross sections vs  $Q^2$